Inorganic Chemistry

ARTICLE

pubs.acs.org/IC

Structural and Electronic Modulation of Magnetic Properties in a Family of Chiral Iron Coordination Polymers

Lihong Li,[†] Jan M. Becker,[†] Laura E. N. Allan,[†] Guy J. Clarkson,[†] Scott S. Turner,*[‡] and Peter Scott*[†]

[†]Department of Chemistry, University of Warwick, Gibbet Hill Road, Coventry CV4 7AL, U.K.

[‡]Department of Chemistry, University of Surrey, Guildford, Surrey GU2 7XH, U.K.

S *Supporting Information*

ABSTRACT: The complexes FeL_2 [**L** = bidentate Schiff base ligands obtained from (*R*)-(+)-α-phenylethanamine and 4-substituted salicylaldehydes, substituent R = H, ^{t}Bu, NO_2, OMe, CN, OH] react with ditopic proligands 1,4-pyrazine (pz) or 4,4′-bipyridine (bpy), to give a family of optically pure Fe(II) polymeric chain complexes of formula $\{FeL_2(\mu\text{-pz})\}_\infty$ and $\{FeL_2(\mu\text{-bpy})\}_\infty$. Crystallographic studies show that a range of structures are formed including unidirectional and bidirectional linear polymers and canted zigzag chains. Interchain interactions via π-contacts and hydrogen bonding are also observed. SQuID magnetometry studies on all of the complexes reveal antiferromagnetic interactions, the magnitudes of which are rationalized on the basis of substituent electronic properties and bridging ligand identity. For complexes with bridging pz, the antiferromangnetic interaction is enhanced by electron-releasing substituents on the Fe units, and this is accompanied by a contraction in the intrachain distance. For complexes bridged with the longer bpy the intrachain antiferromagnetic couplings are much weaker as a result of the longer intrachain distance. The magnetic data for this series of chain complexes follow a Bonner−Fisher 1D chain model, alongside a zero field splitting (ZFS) model for Fe(II) (S = 2) as appropriate. The intrachain antiferromagnetic coupling *J* values, *g*-factors, and the axial ZFS parameter *D* were obtained.

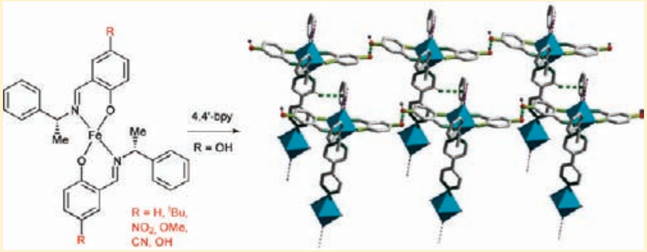

INTRODUCTION

There has been intense interest in molecule-based coordination polymers with one- or multiple-dimensional structures. These may be of use in understanding the fundamental magnetic interactions and magnetostructural correlations in molecular systems and also as new multifunctional molecule-based materials.[1] For instance, applications of coordination polymers have been sought in the areas of nonlinear optical,[2] electrochromic,[3] and multiferroic materials.[4−6] In the approach toward molecule-based magnets, various intermolecular interactions (π-stacking, hydrogen bonding, and van der Waals) are thought to play a role as information transmitters and, therefore, have an important impact on the intermolecular magnetic exchange. The design and characterization of new molecular extended architectures using noncovalent interactions to give predictable physical properties is challenging. In contrast, Olivier Kahn first introduced the idea that direct covalent linking of the active metal sites could increase cooperativity in polymeric compounds with regard to mononuclear ones.[7,8] In this way, small ligands that offer a pathway for magnetic exchange, e.g., cyanide (CN^-),[9,10] oxalate ($C_2O_4^{2-}$),[11−15] azido (N_3^-),[16−20] pyrazine (pz),[21,22] and 4,4′-bipyridine (bpy),[23,24] are responsible for many molecule-based magnets in the literature. These have allowed the engineering of numbers of metal-containing polymers with a large diversity of network topologies, such as one-dimensional molecular chains and ladders, two-dimensional grids and brick-wall structures, and three-dimensional frameworks.[10,18,25−33]

The extension of these concepts to the synthesis of optically pure chiral systems is of current interest because of the possibility of observation of phenomena such as magnetochiral dichroism (MChD)[34] and/or electrical magnetochiral anisotropy (MCA).[35] With this in mind, and with the paucity of opportunities to synthesize a range of systematically related materials, we focused our attention on the reaction of the readily available chiral building blocks FeL_2 (Scheme 1) which we expected to form new coordination polymer systems with bridging ligands such as pz and bpy. The number of comparable systems is rather limited.[36−38] We were particularly interested in being able to make magnetostructural correlations for a family of complexes since general trends and indications for future directions are likely to be a result. In this paper, we report the synthesis, structure, and magnetic properties of eleven Fe(II) chain complexes with general formulas $\{FeL_2(\mu\text{-pz})\}_n$ and $\{FeL_2(\mu\text{-bpy})\}_n$ prepared in this way (Table 1).

RESULTS AND DISCUSSION

Syntheses. We have previously reported the synthesis of several tetrahedral Fe(II) complexes $[FeL^n{}_2]$.[39] The complexes $[FeL^n{}_2]$ (n = 1, 2, 4) are soluble in diethyl ether, and treatment of

Received: November 16, 2010
Published: June 02, 2011

them with pz or bpy in this solvent gave moderate to high yields of highly crystalline and slightly air-sensitive coordination polymers (Scheme 1). The complexes of $\mathbf{L}^3$, $\mathbf{L}^5$, and $\mathbf{L}^6$ are relatively insoluble, and their reactions with the bridging ligands in tetrahydrofuran (THF) gave correspondingly less soluble but crystalline and air-stable materials. We could not isolate a reaction product between [$\mathrm{Fe}\mathbf{L}^6{}_2$] and pz. The structural and magnetic properties of the polymeric products, as determined by single-crystal X-ray diffraction and SQuID magnetometry, are summarized in Table 1. The materials were also characterized by IR, UV/vis, and microanalysis.

Crystal Structures of {$\mathrm{Fe}\mathbf{L}^n{}_2(\mu\text{-Z})\}_\infty$. The Fe-containing units in the following structures usually contain planar *trans*-$\mathrm{Fe}\mathbf{L}_2$ moieties, and as a result the faces presented to incoming ligands are enantiotopic, as we described recently.[39] However, all such planar centers in this study are symmetrically substituted by bridging ligands, so—ignoring the inherent lack of mirror symmetry implied by the chiral side chains—no new stereogenic center is created on formation of the polymer. It remains however that we need to define directionality (i.e., the relative directions of these enantiotopic faces in the polymer). We will thus refer to the “clockwise” and “anticlockwise” (*C* and *A*) faces as defined by an application of the CIP priorities (Figure 1a). Notably the phenyl substituents are usually arranged about the *A* face (Figure 1b), whereas the *C* face is relatively unencumbered.

Scheme 1. Synthesis of Coordination Polymers[a]

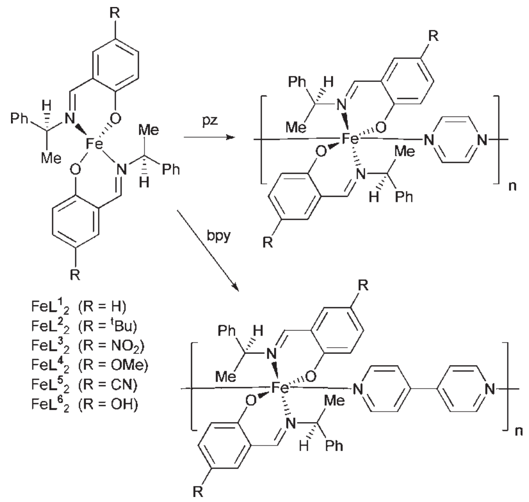

[a] The structures shown represent stoichiometry and the actual crystal structures vary considerably (vide infra).

The asymmetric unit of $\{\mathrm{Fe}\mathbf{L}^1{}_2(\mu\text{-pz})\}_\infty$ contains a trimer with three independent $\mathrm{Fe}\mathbf{L}^1{}_2$ units and three pyrazine ligands (Figure 2). The unit at Fe(2) has the conventional all-trans structure with two bidentate salicyaldiminato ligands occupying the meridional plane. The rotational orientations of the phenethyl groups in this monomer unit are unique in this study (vide infra) in that they point in opposite directions along the chain (as shown in Figure 1d). Nevertheless, the *A* face of the Fe(2) unit is pointing to the right in Figure 2. The axial positions of Fe(2) are occupied by coordinated pyrazines with an angle N(9)−Fe(2)−N(6) of ca. 179.1°. In contrast to this trans Fe(2) which generates a local linear architecture, the Fe(1) and Fe(3) centers produce “corners” via their chiral cis-α configurations [N(10)−Fe(3)−N(1) and N(5)−Fe(1)−N(2) of 86.1 and 87.1° respectively]. {Interestingly they are of opposite helicity (absolute configuration): Λ for Fe(3) and Δ for Fe(1). As we have previously noted, this type of ligand is poorly effective in determining diastereoselection at octahedral centers,[39] although this is the first time we have observed the presence of two absolute configurations at Fe in the same crystal.} The rotational orientations of the Fe(3) and Fe(1) units about the notional Fe(1)−Fe(2)−Fe(3) axis facilitate the formation of two triple $\pi-\pi$ stacks in the asymmetric unit (the centroid−centroid distance is 3.527 Å), which direct the N(1) and N(2) pyrazine bridges “down” and “up” as shown in Figure 2. The torsional angle N(1)−Fe(3)−Fe(1)−N(2) thus created is ca. 180° so that the extended structure of this single chain describes an achiral (i.e., planar 2D) zigzag. Additionally, there are edge-face contacts showing as brown dashed lines. The unit cell however contains two symmetry-related chains (Figure 3a), and the angle between the planes of these zigzag chains is ca. 49° (Figure 3b).

For $\{\mathrm{Fe}\mathbf{L}^1{}_2(\mu\text{-bpy})\}_\infty$ there are two crystallographically independent six-coordinate Fe complex units Fe(1) and Fe(2) (Figure 4a). The Fe atoms and bpy N atoms of each polymer lie on the 2-fold axis on special positions *a* and *b*.[40] The salicyaldiminato ligands are again observed to have the trans arrangement, and the angles subtended by bpy N donor atoms are all close to 180°. The difference in the two polymer chains arises in the directionality of the enantiotopic faces of the planar *trans*-$\mathrm{Fe}\mathbf{L}^1{}_2$ moieties in relation to the *b* axis of the crystal. In the Fe(2) chain

Table 1. Properties of the Coordination Polymers $\{\mathrm{Fe}\mathbf{L}^n{}_2(\mu\text{-Z})\}_\infty$ [Z = 1,4-Pyrazine (pz), 4,4′-Bipyridine (bpy)]

$\mathbf{L}^n$	R	bridge	structure	space group	d_1 [a]/Å	d_2 [b] /Å	Θ [c]/K	intrachain *J*/(cm^{-1})	*C*/(cm^3 K mol^{-1})	maximum in χ_m/K	*D*/cm^{-1}	*g*-factor
$\mathbf{L}^1$	H	pz	Figures 2 and 3	C2	7.3229(10)	12.40	−13.72	−2.44	3.600	14		2.20
		bpy	Figure 4	C2	11.5749(2)	7.45	−0.06	–	3.231	–	10.2	2.10
$\mathbf{L}^2$	ᵗBu	pz	Figure 5	C2	7.3012(23)	12.40	−16.06	–	3.773	–	38.5	2.14
		bpy	–	–	–	–	−0.23	–	3.207	–	11.5	2.10
$\mathbf{L}^3$	NO_2	pz	Figure 6	P2(1)	7.3694(6)	10.33	−5.67	–	3.453	–	21.0	2.10
		bpy	Figure 7	P2	11.6027 (2)	9.08	−7.55	–	3.602	–	10.2	2.06
$\mathbf{L}^4$	OMe	pz	–	–	–	–	−18.72	−3.85	3.056	19		2.14
		bpy	–	–	–	–	−3.33	−0.72	3.610	3		2.16
$\mathbf{L}^5$	CN	pz	–	–	–	–	−7.59	−1.66	3.317	7		2.20
		bpy	Figures 8 and 9	P2(1)2(1)2	11.5590(1)	8.06	−5.88	–	3.680	–	10.5	2.15
$\mathbf{L}^6$	OH	bpy	Figure 10	P1	11.6927(3)	6.58	−0.81	–	3.423	–	12.9	2.12

[a] d_1 = intrachain Fe−Fe distance. [b] d_2 = shortest interchain distance. [c] Θ = Weiss constant.

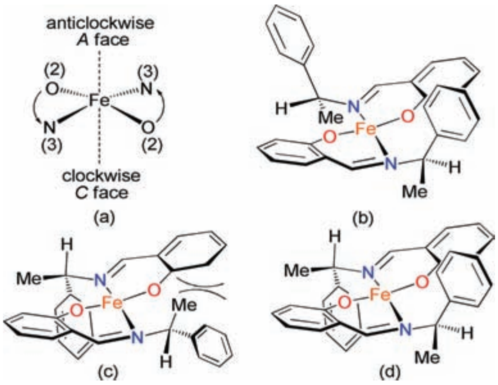

Figure 1. (a) Derivation of the clockwise *C* and anticlockwise *A* descriptors of the enantiotopic faces of planar region of the *trans*-Fe$\mathbf{L}_2$ units; (b) how the phenyl substituents surround the *A* face in the more commonly observed orientation; (c) the less frequently observed, more sterically compressed orientation; (d) a hybrid structure observed only in $\{\mathrm{Fe}\mathbf{L}^1{}_2(\mu\text{-pz})\}_\infty$.

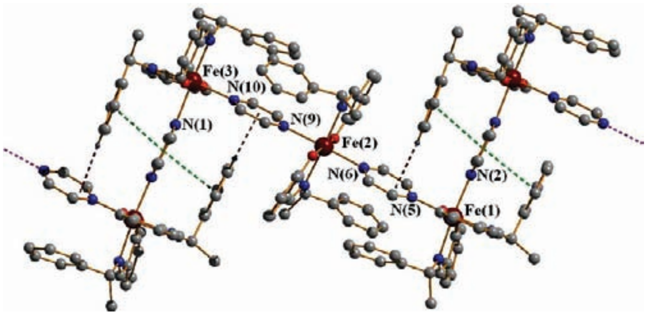

Figure 2. $\{\mathrm{Fe}\mathbf{L}^1{}_2(\mu\text{-pz})\}_\infty$ showing triple $\pi-\pi$ stacking (green dashed lines) and edge-face stacking (brown dashed lines).

traveling along the 2-fold axis on special position *a*, the *A* face (vide supra) points up the *b* axis of the cell (i.e., to the left in Figure 4a). In the Fe(1) chain running along the 2-fold axis on special position *b*, the *A* face points down the *b* axis of the cell (i.e., to the right). The orientations of the imine phenethyl groups are all conventional (Figure 1b), and thus the two phenyls of each *trans*-Fe$\mathbf{L}^1{}_2$ unit surround the pyridyl ring at the enantiotopic *A* face, and the methyls align themselves around the *C* face. There are edge-face interactions between a bpy bridging ligand from one chain and a benzyl group from another chain in the asymmetric unit (brown dashed lines) so that the side chains are interdigitated. This allows close approach of the main chains at 7.45 Å (Figure 4b).

In $\{\mathrm{Fe}\mathbf{L}^2{}_2(\mu\text{-pz})\}_\infty$ there are also two crystallographically independent chains in the asymmetric unit (interchain distance is 12.40 Å; see Supporting Information section S1), one with repeat unit Fe(1)−Fe(2)−Fe(3) and one Fe(4)−Fe(5)−Fe(6). The chains lie on the 2-fold axes with the 4-*tert*-butylsalicyaldiminato ligands adopting a trans orientation and the Fe and pyrazine N atoms lying on the 2-fold axis. The three complexes that form the repeat unit of each polymeric chain do not have the same directionalities; for example the *C* faces of Fe(1) and Fe(3) are oriented in the positive direction of the *b* axis (right to left in Figure 5), whereas for Fe(2) it is the *A* face. At the same time, the orientation of the phenethyl units in Fe(1) is the more sterically compressed type of Figure 1c with the phenyl groups surrounding the *C* face. Overall this leads to substantial differences in the environments of the bridges. Pyrazine N(8)−N(7) is surrounded by four phenyl groups from neighboring complex units, and pyrazine N(5)−N(4) is surrounded by two phenyl groups, while pyrazine N(2)−N(1) has only neighboring acetonitrile solvent. In the Fe(4)−Fe(5)−Fe(6) chain no solvent was located in this region. This sterically unencumbered pyrazine bridge is also unique in that it is tilted out of the near copolymer arrangement of the other pyrazine bridges. The *tert*-butyl groups of the ligands on alternate complexes of the polymer chain are roughly orthogonal except on either side of the sterically unencumbered pyrazine bridges where they are eclipsed (torsion angle N(3)−Fe(1)−Fe(3)−N(9) is 1.3°).

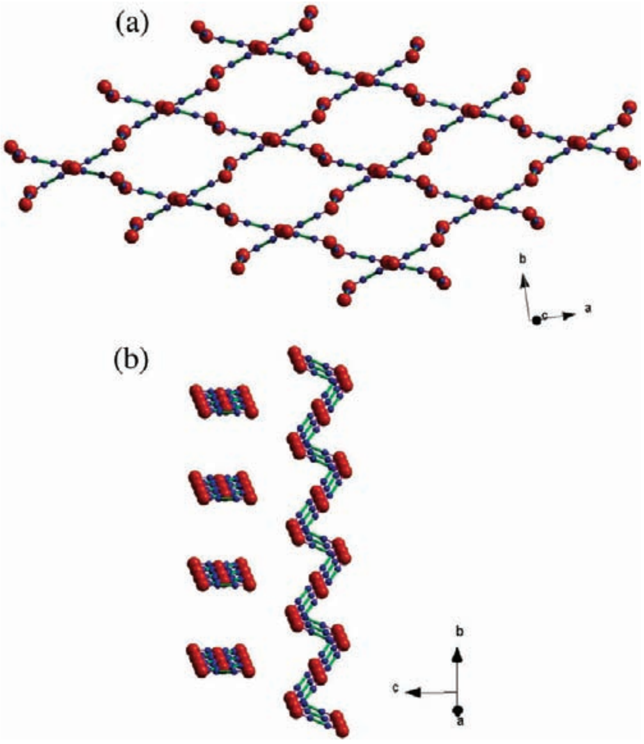

Figure 3. Two symmetry-related chains in crystals of $\{\mathrm{Fe}\mathbf{L}^1{}_2(\mu\text{-pz})\}_\infty$: (a) showing the angle between the planes of the zigzag chains (ca. 49°; red spheres represent Fe atoms, and smaller blue spheres represent pyrazine N atoms); (b) with chains projecting into the page and in the plane of the page.

The asymmetric unit of complex $\{\mathrm{Fe}\mathbf{L}^3{}_2(\mu\text{-pz})\}_\infty$ contains the Fe$\mathbf{L}^3{}_2$ complex and a pz bridging ligand (Figure 6a). The complex forms a simple 1D chain traveling parallel to the *a* axis of the cell. The *C* enantiotopic face of each Fe$\mathbf{L}^3{}_2$ complex points the same way along the polymer backbone. There is a symmetry-related chain facing the opposite direction in the unit cell related by the 2(1) screw axis (see Supporting Information), and this results in the shortest interchain axis distance of 10.33 Å for this particular material (Table 1). The 4-nitrosalicyaldiminato ligands are all aligned (eclipsed) along the polymer backbone, and the pz bridges all lie in the same plane (Figure 6b). There is a $\pi-\pi$ stacking interaction between one of the benzyl groups of the ligands and the bridging pyrazine with the centroid−centroid distance of ca. 3.607 Å and an angle between planes of interacting π-systems of ca. 9.67° (Figure 6b). Additionally, each nitro group is sandwiched between the aromatic rings of the nitrophenyls of a neighboring chain so that the chains are interdigitated. The NO_2 groups extend far enough into the sandwich to have a relatively

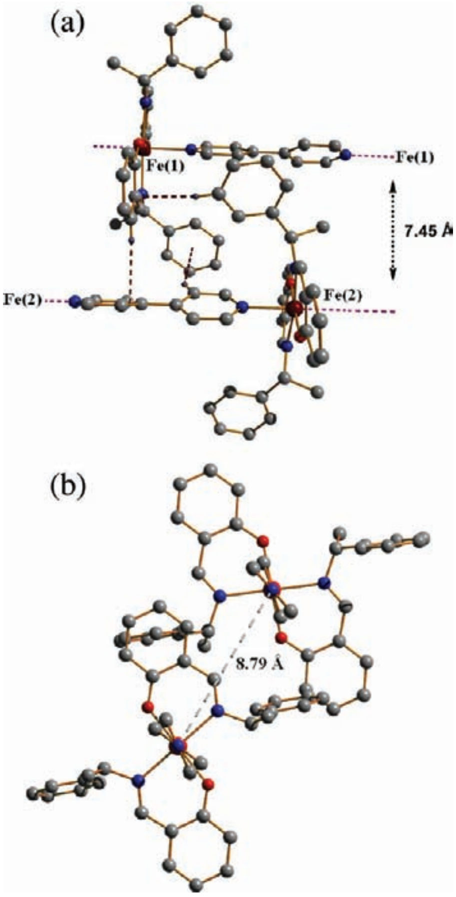

Figure 4. Structure of asymmetric unit in $\{\mathrm{Fe}\mathbf{L}^1{}_2(\mu\text{-bpy})\}_\infty$: (a) shown with edge-face interactions (brown dashed line) between two benzyl groups from two adjacent chains; (b) viewed along the chains showing shortest interchain Fe−Fe distance. (Hydrogens and solvent have been removed for clarity.)

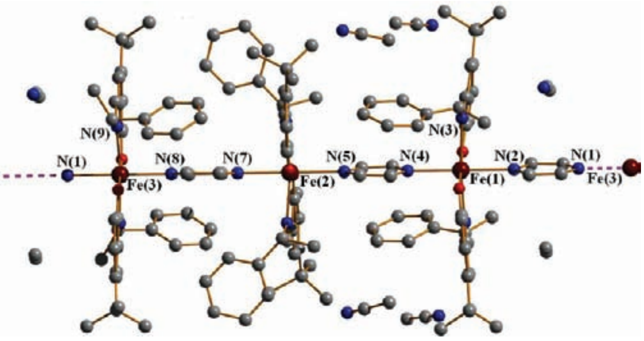

Figure 5. Polymeric chain structure for $\{\mathrm{Fe}\mathbf{L}^2{}_2(\mu\text{-pz})\}_\infty$. (Hydrogens have been removed for clarity.)

close contact with the H atoms of the pyrazine bridges (the closest contact = 2.59 Å).

The asymmetric unit of $\{\mathrm{Fe}\mathbf{L}^3{}_2(\mu\text{-bpy})\}_\infty$ contains two polymeric complexes that lie on the 2-fold axis (Figure 7) and several molecules of THF. The Fe(1) complex lies on the 2-fold axis on special position *d*[40] running through the center of the cell and the Fe(2) polymer lies on the special postion *a* where the 2-fold axis runs along the *b* axis of the cell. The *trans*-4-nitrosalicyaldiminato ligands of each $\mathrm{Fe}\mathbf{L}^3{}_2$ unit are aligned along the polymer backbone. Each bridging bpy ligand has an identical orientation with a dihedral angle between the pyridine rings of 26.6° in the Fe(1) polymer and 39.0° in the Fe(2) polymer. The *A* enantiotopic faces of the Fe(1) chain face up the *b* cell axis, whereas for Fe(2) it is the *C* face.

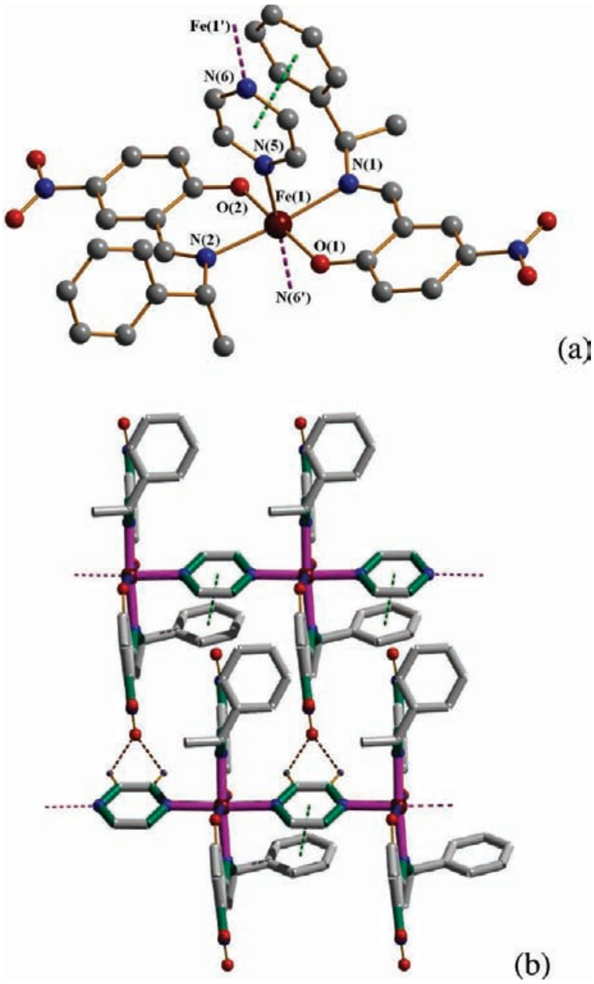

Figure 6. Structure of $\{\mathrm{Fe}\mathbf{L}^3{}_2(\mu\text{-pz})\}_\infty$; (a) asymmetric unit; (b) unidirectional chains showing $\pi-\pi$ stacking between benzyl ring and bridging pyrazine ligand. (Hydrogen atoms and solvent acetonitrile have been removed for clarity.)

In both polymers, the pyridinyl unit at the *A* face of the $\mathrm{Fe}\mathbf{L}^3{}_2$ unit is surrounded by the two aromatic rings of the phenethyl substituents of that complex (Figure 7). In the Fe(2) chain, the angle between the phenethyl rings and the pyridine ring of the bpy bridge is 64.9° with a CH−π interaction between a phenethyl aromatic CH and the pyridine ring (CH−pyridine ring centroid, ca. 2.852 Å). In the Fe(1) polymer, the angle between the phenethyl aromatics and the bridging pyridine is much more acute at 29.2° but with little overlap that could indicate π stacking. Accompanying this is however edge-face short contact between the nitroarene from the Fe(2) chain and pyrazine ring from the Fe(1) chain. The distance between these two chains is 9.08 Å.

The asymmetric unit of $\{\mathrm{Fe}\mathbf{L}^5{}_2(\mu\text{-bpy})\}_\infty$ contains two independent monomer units at Fe(1) and Fe(2) which form chains running in opposite directions. In the structures described earlier

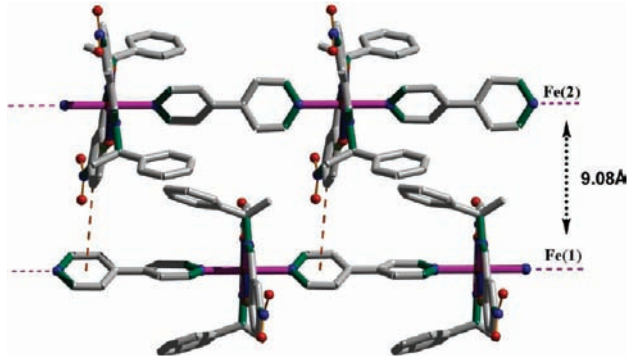

Figure 7. Alternating directions of neighboring chains in $\{FeL^3_2(\mu\text{-bpy})\}_\infty$ showing edge-face interactions (brown dash lines). (Hydrogen atoms and solvent THF removed for clarity.)

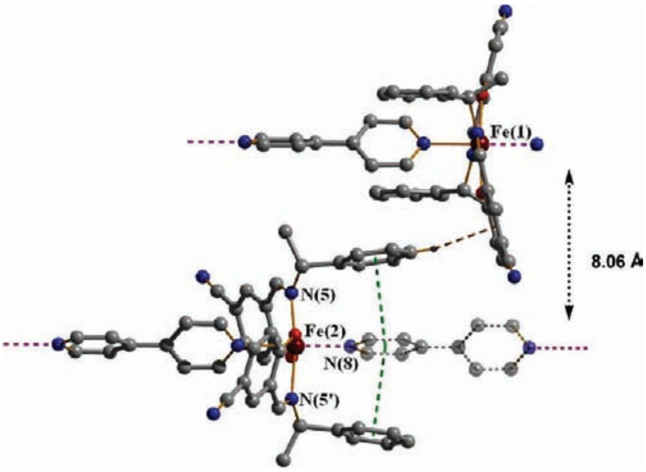

Figure 8. Asymmetric unit for $\{FeL^5_2(\mu\text{-bpy})\}_\infty$ showing triple $\pi-\pi$ stacking (green dash lines) and edge-face contact (brown dash lines). (Hydrogen atoms and solvent $CHCl_3$ have been removed for clarity.)

the mean planes of the salicyl arene units are close to orthogonal to the polymer axis, and the angles between these planes are usually <10°. In the Fe(2) chain here there is a substantial distortion, creating a bowl around the *C* enantiomeric face of the complex unit; the angle between the two salicyl arene planes (i.e., at the base of the bowl) is ca. 112°. This is accompanied by an unusually large distortion from octahedral in the first coordination sphere at Fe(2) [with the angle N(5)−Fe(2)−N(5′) rather low at 171.8(10)°] and the formation of a triple $\pi-\pi$ stack between the two phenethyl groups and the bpy ring at N(8) outside the bottom of the bowl. The angle between mean planes defined by the two symmetry-related phenethyl aromatic rings and the pyridinyl unit is 9.25° with the shortest interatomic contact 3.32 Å. At the Fe(1) centers there is also a significant bowl distortion with the same orientation as at Fe(2), but it is less pronounced, and the angle between salicyl arene planes is 153°.

Figure 8 also indicates short edge-face interactions formed between the chains. Nearest neighbor chain axes are ca. 8.06 Å apart with a more distant approach of 10.53 Å. The longer interchain distance is also indicated in Figure 9, which shows how the relative orientations of the chains and in particular the lateral "shift" between chains positions in the crystal.

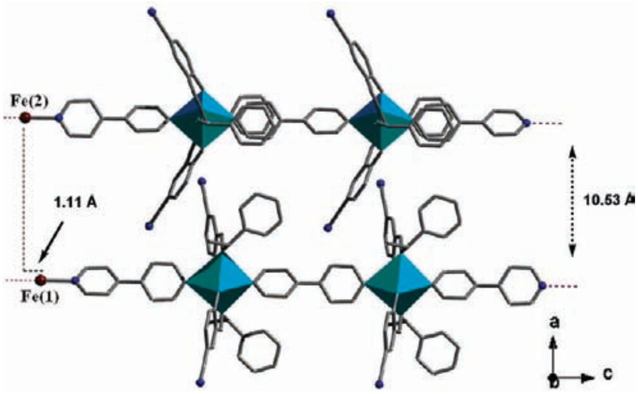

Figure 9. Showing the longer interchain distance and lateral shift between Fe atoms in adjacent chains in $\{FeL^5_2(\mu\text{-bpy})\}_\infty$.

The compound $\{FeL^6_2(\mu\text{-bpy})\}_\infty$ comprises linear chains all oriented in the same direction. The dihedral angle between mean planes through the pyridinyl units of the bridging ligand is ca. 31.6°. The aromatic rings of the phenethyl substituents have no strong intramonomer interactions with the bridge, but there are many contacts with neighboring polymer chains. The monomers lie in the plane of a hydrogen bonded network formed by the OH groups (Figure 10b). These hydrogen bonded contacts are complemented by several CH−π interactions between the neighboring chains involving the phenethyl aromatic rings, the salicyl rings and the bpy ligand, and range from 2.4 to 3.4 Å in the CH to ring centroid distance. Although the intrachain Fe−Fe distances are governed by the length of the bridging bpy ligand, this compound has the shortest interchain Fe−Fe distance at 8.7967(2) Å (interchain axis distance d_2 of 6.58 Å). Additionally, there is a much longer interchain distance of 14.89 Å between pairs connected by hydrogen bonds.

Magnetic Measurements. The magnetic properties of the present series of compounds were investigated on polycrystalline samples using SQuID magnetometry. In this section we will describe trends in the magnetic properties that relate to the nature of the bridging group, interchain distances, and electronic properties of the Fe complex units arising from the ligand substituents.

For mononuclear iron(II) complexes with a regular octahedral crystal field, the $^5T_{2g}$ ground term has first-order spin−orbit coupling contribution (with a spin−orbit parameter λ of about $-100\ cm^{-1}$) which removes the degeneracy of the electronic ground states and may cause magnetic anisotropy. In this case, the average susceptibility may not follow the Curie−Weiss law, particularly at low temperatures.[1] The presence of four unpaired electrons ($S = 2$), together with the imposed distortion from O_h symmetry, results in the $^5T_{2g}$ term splitting into the $^5B_2$ and ^5E multiplets, or a zero-field splitting (ZFS).[1] For an isolated Fe(II) ion, a spin only $\chi_M T$ value of 3.001 $cm^3\ K\ mol^{-1}$ (when $g = 2$; χ_M is molar magnetic susceptibility) would be expected at room temperature, which should remain constant as temperature is lowered. However, due to the presence of either ZFS, antiferromagnetic interactions, or spin crossover (SCO),[41] the experimental magnetic moments can be lower than this value.[42]

Because spin−orbit coupling contributes significantly for regular octahedral complexes and ZFS contributes more when there is a strong distortion in the regular geometry, the magnetic behavior for mononuclear Fe(II) complexes will depend on the

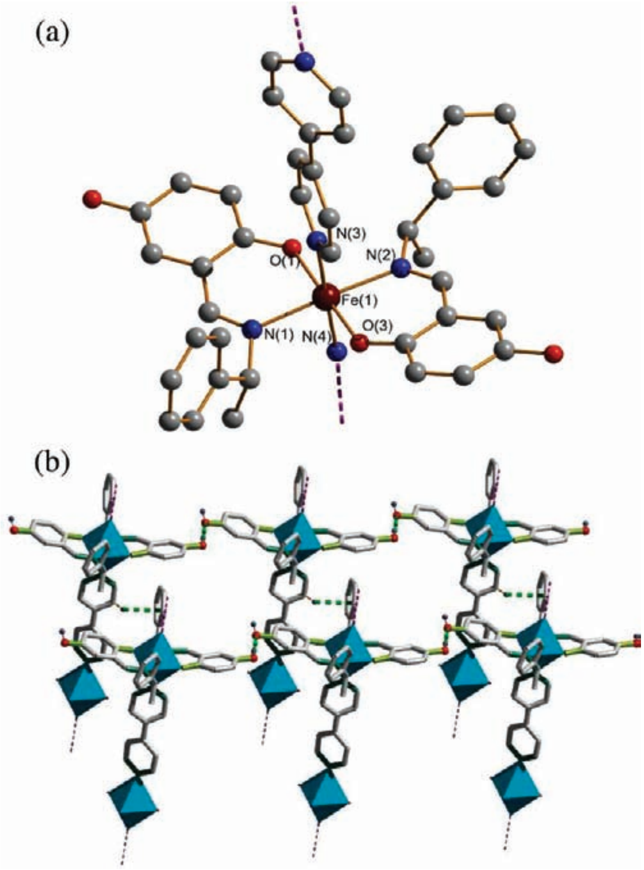

Figure 10. (a) Asymmetric unit of $\{FeL^6{}_2(\mu\text{-bpy})\}_\infty$; (b) interchain hydrogen bonds and edge-face CH···π contacts in $\{FeL^6{}_2(\mu\text{-bpy}.$ (Hydrogens and solvent molecules have been removed for clarity.)

Scheme 2. Schematic Representation of the Intrachain Coupling[a]

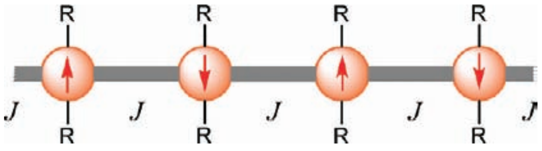

[a] J is the antiferromagnetic coupling constant, and R is the substituent on ligand **L**$''$ (Scheme 1). Circles represent the paramagnetic metal complex units Fe**L**$''_2$.

geometry. Further complication arises when there is the possibility of exchange-coupled transition-metal ions, as in the coordination polymers we present here (Scheme 2). When the Fe(II) magnetic centers are bridged with either pz or bpy, the magnetic coupling between the two nearest spin carriers is expected to be antiferromagnetic. To study these systems, we have modeled the high-temperature data (>ca. 50 K) with the Curie−Weiss law, in order to determine the magnitude of short-range coupling. For some compounds a slightly modified Curie−Weiss equation has been used which takes into consideration a small temperature-independent paramagnetic term. In addition we have applied a model covering the whole temperature range, which depends on the form of the data. Some compounds clearly show a maximum in the χ_M vs T data. For these we have assumed

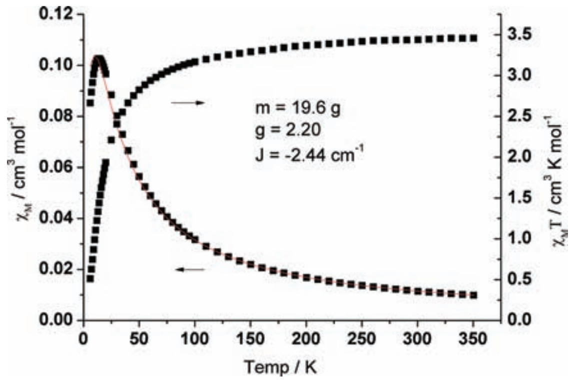

Figure 11. χ_M and $\chi_M T$ vs T for $\{FeL^1{}_2(\mu\text{-pz})\}_\infty$ with fitting to the Bonner−Fisher equation.

a 1D chain structure and applied the Bonner−Fisher equation (eq 1) for a $S = 2$ system in order to extract J and g values.[43]

$$\chi_M = \frac{Ng^2\beta^2 S(S+1)}{3kT}\,\frac{1+u}{1-u} \tag{1}$$

where

$$u = \coth\left[\frac{JS(S+1)}{kT}\right] - \left[\frac{kT}{JS(S+1)}\right]$$

The remaining compounds do not have a maximum in χ_M but do have a sharp downturn in $\chi_M T$, at low temperature, and we have assumed the effect is a result of ZFS. For these cases we have applied a ZFS model for d^6 high-spin octahedral species (eq 2), to extract g and D, the axial ZFS parameter.

$$\chi_M = (\chi_\parallel + \chi_\perp)/3 \tag{2}$$

where

$$\chi_\perp = \frac{Ng^2\beta^2}{kT}\left(\frac{2\exp(-A) + 8\exp(-4A)}{1 + 2\exp(-A) + 2\exp(-4A)}\right)$$

$$\chi_\parallel = \frac{Ng^2\beta^2}{kT}\left(\frac{(6A^{-1})(1-\exp(-A)) + ((4/3)A^{-1})(\exp(-A)+\exp(-4A))}{1 + 2\exp(-A) + 2\exp(-4A)}\right)$$

$$\text{and}\quad A = \frac{D}{kT}$$

Table 1 summarizes the parameters obtained from least-squares fitting to the above equations. In the following discussion two specific examples are described that illustrate how the fitting equations have been used, followed by an analysis of general trends. Further specific data and descriptions are included in the Supporting Information.

Figure 11 shows curves of χ_M, and $\chi_M T$ vs T for $\{FeL^1{}_2(\mu\text{-pz})\}_\infty$. From 350 K, the molar susceptibility χ_M increases smoothly with decreasing temperature, passing through a rounded maximum at 14 K, and then decreases to the base temperature. The value of $\chi_M T$ decreases gradually from room temperature (3.438 cm^3 K mol^{-1}) to 70 K (3.016 cm^3 K mol^{-1}) and then drops rapidly to 0.512 cm^3 K mol^{-1}. Such behavior is typical of intrachain antiferromagnetic order. A least-squares fit to the Bonner−Fisher equation gives $J = -2.44$ cm^{-1} and $g = 2.20$ (solid line in Figure 11). The inverse molar susceptibility $\chi_M{}^{-1}$ vs T for $\{FeL^1{}_2(\mu\text{-pz})\}_\infty$ is given in Figure 12, and fitting to

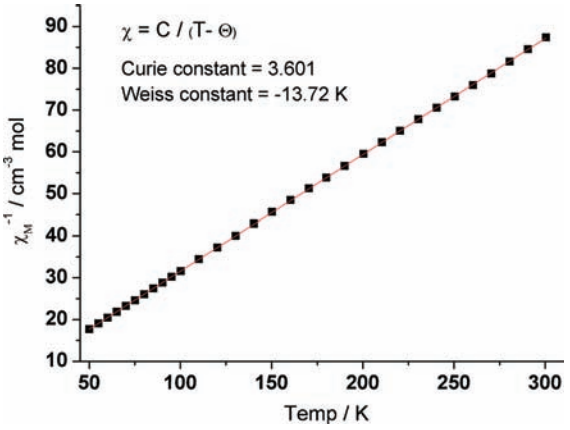

Figure 12. χ_M^{-1} vs T for $\{FeL^1{}_2(\mu\text{-pz})\}_\infty$ with fitting to the Curie–Weiss Law.

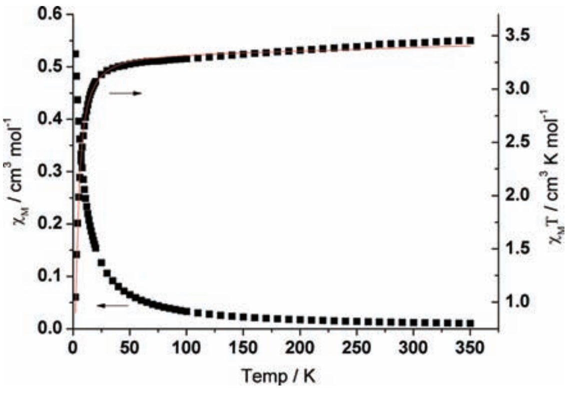

Figure 13. χ_M and $\chi_M T$ vs T for $\{FeL^1{}_2(\mu\text{-bpy})\}_\infty$ with fitting to the ZFS model.

the Curie–Weiss law (solid line) gives a Curie constant of 3.60 and a Weiss constant of −13.72 K.

Curves of χ_M and $\chi_M T$ vs T for $\{FeL^1{}_2(\mu\text{-bpy})\}_\infty$ are shown in Figure 13. The room-temperature $\chi_M T$ value per Fe(II) ion is 3.521 cm^3 K mol^{-1}, which is comparable to the expected spin-only value of 3.372 cm^3 K mol^{-1}, when $S = 2$ and $g = 2.10$ (g is obtained from fitting the data to the ZFS model). The fitting to the ZFS model also gives a value of $D = 10.2$ cm^{-1}. A plot of the inverse molar susceptibility χ_M^{-1} vs T (Figure 14) shows a slight deviation from Curie–Weiss behavior, which was modeled by a modified Curies–Weiss law ($\chi_M = C/(T - \Theta) + \chi_{TIP}$). This gave a Curie constant of 3.23, a Weiss constant of −0.48 K, and a temperature-independent paramagnetic term, χ_{TIP}, of 1.0 × 10^{-5} cm^3 mol^{-1}. Compared to $\{FeL^1{}_2(\mu\text{-pz})\}_\infty$, the intrachain Fe(II)–Fe(II) distance is longer, at 11.5749(2) Å, and there is consequently no observed maximum in χ_M.

For the pz series there is a clear trend in the magnetic data that as the electron releasing power of the substituent R increases ($\mathbf{L^3} < \mathbf{L^5} < \mathbf{L^1} < \mathbf{L^2} < \mathbf{L^6} < \mathbf{L^4}$), the magnitude of Θ increases, consistent with stronger short-range antiferromagnetic interactions between spin centers. While there are some structural differences between compounds in this series—perhaps most importantly the zigzag structure of the $\mathbf{L^1}$ complex—the interchain distances are all relatively large (Table 1) and the intrachain interactions are expected to dominate. In this respect it is noteworthy that the Fe···Fe distances d_1 we have measured

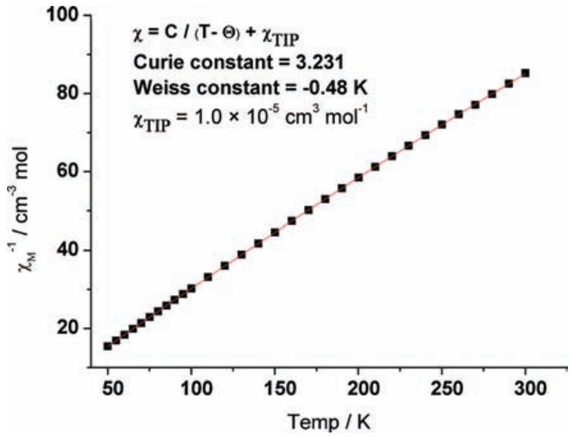

Figure 14. χ_M^{-1} vs T for $\{FeL^1{}_2(\mu\text{-bpy})\}_\infty$ with fitting to the Curie–Weiss Law.

fall off significantly in the same order as above; i.e., $\mathbf{L^3} > \mathbf{L^1} > \mathbf{L^2}$ from ca. 7.37 to 7.30 Å. While this change will contribute to an increased magnetic coupling, we consider that it is insufficient to explain alone the substantial change in Θ. If however we consider the Fe(II) center to be a charge donor and the neutral pz to be a charge acceptor, as we increase the energy of occupied metal orbitals (by increasing the electron-releasing power of the substituent), we expect to improve the energy match between these orbitals and the acceptor orbitals on the pz ligand, and thus facilitate intrachain magnetic coupling.

For the bpy series, the Weiss constants are, as expected, generally lower in magnitude and there is also no consistent trend in the magnetic data with the electronic properties of substituent R. This might be expected on the basis of the longer distances d_1 compared with the pz series, and indeed corresponds with our expectation that if the intrachain Fe···Fe distances are too large to facilitate substantial magnetic coupling, we do not expect a remote electronic property in substituent R to have a significant modulating effect. We note however that while the pz materials have isolated chains (with some small interchain secondary interactions), the bpy systems are characterized by interdigitation of planar FeL_2 units (e.g., Figure 4). This leads to substantially shorter interchain distances d_2. For the four structures available, d_2 falls from ca. 9.1 to 6.6 Å in the order $\mathbf{L^3} > \mathbf{L^5} > \mathbf{L^1} > \mathbf{L^6}$ and Θ increases from −7.6 to −0.8 in the same order. There does therefore seem to be a correspondence between the structural parameter d_2 and the magnetic properties, although of course the effects are weak. It is nevertheless reasonable, given that the interchain distances are becoming rather short, to ascribe this to the onset of interchain magnetic interactions.

■ CONCLUSIONS

We have synthesized 11 new polymeric chain complexes. For seven of these materials we have obtained single-crystal structural data. As a result of the presence of stereogenic centers on the ligands and/or at the metal atoms, a range of structural types and features were observed: simple 1D chains, zigzags, directionality of the enaniotopic faces (Figure 1a), and interchain interations such as H-bonding and arene–arene contacts. We have also investigated their magnetism: For the complexes bridged with 1,4-pyrazine, relatively short intrachain distances between nearest spin carriers generally leads to strong antiferromagnetic behavior via coupling along the chain. Electronic effects also play a role, and electron releasing groups promote this antiferromagnetic interaction in part via the accompanying shortening of intrachain distances but probably also as a result of the increased reducing power of the Fe(II) centers as R becomes more electron-releasing. For complexes with the longer bpy bridge this electronic effect is unimportant, but since there is a trend in the magnetic data with interchain distance, we suggest that structural effects including secondary interactions (π-interactions and H-bonding) may be beginning to play a role.

Overall this study clearly shows how the electronic properties of substituents and the crystal structure can affect magnetism in such extended molecular systems. On this basis we are now making efforts to design new chiral systems that enhance such effects.

■ EXPERIMENTAL DETAILS

General Comments. Where necessary, manipulations were carried out under an inert atmosphere of argon by using a dual manifold vacuum/argon line and standard Schlenk techniques, or in an MBraun Labstar glovebox. All glassware and cannulae were stored in an oven (>373 K). Solvents were predried (where appropriate) over sodium wire and then refluxed for 3 days under dinitrogen over the appropriate drying agents (potassium for THF; sodium−potassium alloy for diethyl ether, hexane, and pentane; magnesium methoxide for methanol; calcium hydride for dichloromethane and acetonitrile). Solvents were stored in glass ampules under argon and degassed before use. The Fe(II) intermediates $\mathrm{Fe}\mathbf{L}_2$ were synthesized according to our published procedures.[39]

Infrared spectra were obtained as Nujol mulls by using a Perkin-Elmer spectrum 100. UV/vis spectra were obtained as acetonitrile solutions in a quartz cell of path length 0.1 cm, using a Jasco V-660 spectrometer. Elemental analyses were performed by Warwick Analytical Services or Medac Analytical Ltd., Surrey.

Crystallography. Crystals were coated in inert oil prior to transfer to a cold nitrogen gas stream on an Oxford Diffraction Gemini four-circle system with Ruby CCD area detector and held at 100(2) K with the Oxford Cryosystem Cryostream Cobra. Structures were solved by direct methods (SHELXTL) with additional light atoms found by Fourier methods (Table 2). All non-hydrogen atoms were added at calculated positions and refined using a riding model.

In $\{\mathrm{Fe}\mathbf{L}^3{}_2(\mu\text{-bpy})\}_\infty$ one THF molecule O(100) was refined as fully occupied. One fully occupied THF was modeled as disordered over two positions O(200)−C(204) and C(20A)−C(24A) in a 50:50 ratio. The position of the oxygen in the latter could not be determined. THF O(300) was modeled as half-occupied and lies on a 2-fold axis (but has no atoms on the axis). The disorder was modeled as a pucker in the ring related by the 2-fold axis. The atom in the pucker was modeled as the oxygen O(300). THF C(400) was modeled as half-occupied with the 2-fold axis running through the THF and C400 lying on the 2-fold axis. The oxygen position could not be determined. The formula for the cell contents has been modified to reflect the actual contents of the cell so as to calculate the correct density as no hydrogens were added to the minor component THF molecules and the assignment of their oxygen atoms could not be determined. These partially occupied and disordered THFs were refined isotropically.

Crystals of $\{\mathrm{Fe}\mathbf{L}^1{}_2(\mu\text{-pz})\}_\infty$ were weakly diffracting and restraints were used to give the two diethyl ether molecules chemically reasonable bond lengths, angles, and thermal parameters. Restraints were also used on the large thermal parameters of the outer carbons of phenylimine ligands. The structure contains large voids. The Squeeze program (run via Platon) calculates 748 Å^3 of solvent accessible void. There were no major peaks left in the difference map, and elemental analysis does not indicate any further solvent included.

In $\{\mathrm{Fe}\mathbf{L}^3{}_2(\mu\text{-pz})\}_\infty$ the asymmetric unit contains a partially occupied molecule of acetonitrile which was modeled as 75% occupied. Crystals were very thin (less than 0.01 mm) and poorly diffracting.

Crystals of $\{\mathrm{Fe}\mathbf{L}^1{}_2(\mu\text{-bpy})\}_\infty$ and $\{\mathrm{Fe}\mathbf{L}^5{}_2(\mu\text{-bpy})\}_\infty$ had no meaningful diffraction above 62°. Many alternative crystals were investigated. In the latter a molecule of chloroform contained in a cavity between the polymer chains was modeled as disordered over two positions and refined to a ratio of 75:25. The minor component chloroform was refined isotropically.

The unit cell of $\{\mathrm{Fe}\mathbf{L}^6{}_2(\mu\text{-bpy})\}_\infty$ contains two molecules of THF. One was modeled as disordered over two positions O(201)−C(205) and O(201)−C(305) and refined to a ratio of 54:46. Several restraints were required to give all the THFs chemically sensible bond lengths and thermal parameters.

Crystals of $\{\mathrm{Fe}\mathbf{L}^2{}_2(\mu\text{-pz})\}_\infty$ were weakly diffracting. The asymmetric unit contains three molecules of acetonitrile that were each refined at 75% occupancy. There is a pseudocenter of inversion that relates over 80% of the atoms of the two polymeric chains with the only variation around the stereogenic centers. Restraints were needed to make the thermal parameters of many of the atoms chemically sensible, especially the tertiary butyl groups which are undergoing large thermal libration. The structure also contains large voids. The Squeeze program (run via Platon) calculates 884 Å^3 of solvent accessible void. There were no major peaks left in the difference map.

SQuID Measurements. Measurements were made with a Quantum Design MPMS-5 SQuID magnetometer in the temperature range of 2−350 K. Samples were randomly orientated powders in Kel-F capsules. The direct current (DC) measurements were carried out in an external magnetic field of 1000 Oe in warming mode. The capsule was centered using a pure Ni sample. The data were then corrected for the measured diamagnetism of the capsule and the diamagnetic contributions of the sample using Pascal's constants.[44]

[$\{\mathbf{FeL^1{}_2}(\mu\text{-}\mathbf{pz})\}_\infty$]. To a solution of [$\mathrm{Fe}\mathbf{L}^1{}_2$] (0.252 g, 0.5 mmol) in diethyl ether (10 mL) was added pyrazine (0.04 g, 0.5 mmol) in diethyl ether (10 mL). The mixture was then allowed to stir overnight. The solvent was removed in vacuo to induce crystallization. The product was isolated by filtration (0.19 g, 65%). Single crystals were grown in diethyl ether/MeOH at −5 °C. IR (cm^{-1}): 1598 s, 1537 m, 1414 w, 1401 w, 1346 m, 1131, 1196, 1148, 1038, 968, 917, 885, 847, 756 w, 736 m, 697 m. Anal. Found (calcd for $C_{34}H_{32}FeN_4O_2$; %): C, 69.67 (69.87); H, 5.48 (5.52); N, 9.52 (9.59). UV in MeCN (λ, nm (ε, M^{-1} cm^{-1})): 234 (54 000), 260 (38 000), 352 (17 000), 500 (5000).

[$\{\mathbf{FeL^1{}_2}(\mu\text{-}\mathbf{bpy})\}_\infty$]·$\mathbf{CH_3OH}$. To a solution of [$\mathrm{Fe}\mathbf{L}^1{}_2$] (0.252 g, 0.5 mmol) in methanol (10 mL) was added 4,4′-bipyridine (0.08 g, 0.5 mmol) in methanol (10 mL). The mixture was then allowed to stir overnight. The solvent was removed in vacuo to induce crystallization. The product was isolated by filtration (0.26 g, 75%). Single crystals were grown by slow cooling of a hot acetonitrile solution. IR (cm^{-1}): 1597, 1535, 1342, 1261, 1213, 1147, 1094, 1028, 799, 721, 667 w. Anal. Found (calcd for $C_{41}H_{40}FeN_4O_3$; %): C, 70.96 (71.10); H, 5.49 (5.82); N, 8.07 (8.09). UV in MeCN (λ, nm (ε, M^{-1} cm^{-1})): 236 (52 000), 267 (30 000), 350 (16 000), 500 sh (6000)

[$\{\mathbf{FeL^2{}_2}(\mu\text{-}\mathbf{C_4H_4N_2})\}_\infty$]. To a stirred solution of [$\mathrm{Fe}\mathbf{L}^2{}_2$] (0.308 g, 0.5 mmol) in Et_2O (20 mL) was added a colorless solution of pyrazine (0.04 g, 0.5 mmol) in Et_2O (10 mL) via cannula. The mixture was stirred for 15 min and concentrated to ca. 5 mL. Single crystals were grown in acetonitrile upon standing at −5 °C for 1 week (0.23 g, 66%). IR (cm^{-1}): 1613 m, 1531 w, 1462 s, 1414 w, 1377 m, 1328, 1269, 1177, 1073, 1037, 829, 721, 697 w. Anal. Found (calcd for $C_{42}H_{48}FeN_4O_2$; %): C, 72.14 (72.41); H, 7.14 (6.94); N, 7.85 (8.04). UV in MeCN (λ, nm (ε, M^{-1} cm^{-1})): 235 (85 000), 364 (20 000), 488 sh (5000).

Table 2. Crystallographic Data, Collection Parameters, and Refinement Parameters for $\{\mathrm{FeL}^{n}{}_2(\mu\text{-Z})\}_\infty$

	$[\{\mathrm{FeL}^1{}_2(\mu\text{-pz})\}_\infty]_3(\mathrm{Et_2O})_2$	$[\{\mathrm{FeL}^1{}_2(\mu\text{-bpy})\}_\infty]_2(\mathrm{MeCN})_2$	$[\{\mathrm{FeL}^2{}_2(\mu\text{-pz})\}_\infty]_3(\mathrm{MeCN})_{2.25}$	$[\{\mathrm{FeL}^3{}_2(\mu\text{-pz})\}_\infty](\mathrm{MeCN})_{0.75}$	$[\{\mathrm{FeL}^3{}_2(\mu\text{-bpy})\}_\infty](\mathrm{THF})_{2.5}$	$\{\mathrm{FeL}^5{}_2(\mu\text{-bpy})\}_\infty\mathrm{CHCl_3}$	$[\{\mathrm{FeL}^6{}_2(\mu\text{-bpy})\}_\infty](\mathrm{THF})_2$
empirical formula	$C_{110}H_{116}Fe_3N_{12}O_8$	$C_{44}H_{42}$ FeN_6O_2	$C_{130}H_{150.75}Fe_3N_{14.25}O6$	$C_{35.50}H_{32.25}FeN_{6.75}O_6$	$C_{50}H_{54}FeN_6O_{8.50}$	$C_{43}H_{35}Cl_3FeN_6O_2$	$C_{48}H_{52}FeN_4O_6$
FW	1901.70	742.69	2182.45	705.28	930.84	829.97	836.79
cryst size (mm)	0.30 × 0.12 × 0.12	0.20 × 0.10 × 0.08	0.20 × 0.10 × 0.06	0.25 × 0.03 × 0.01	0.40 × 0.18 × 0.02	0.20 × 0.10 × 0.06	0.30 × 0.20 × 0.10
cryst syst	monoclinic	monoclinic	monoclinic	monoclinic	monoclinic	orthorhombic	triclinic
space group	C_2	C_2	C_2	$P2_1$	$P2$	$P2_12_12$	$P1$
a/Å	28.9533(7)	26.8700(6)	25.4871(8)	7.3694(6)	13.3100(3)	21.05493(13)	8.7967(2)
b/Å	13.0045(3)	11.5749(2)	21.9537(8)	19.797(3)	11.6027(2)	16.11390(10)	8.9245(2)
c/Å	26.7340(8)	14.8955(3)	24.8107(11)	12.13478(18)	15.9378(4)	11.55863(8)	14.7428(4)
α/deg	90	90	90	90	90	90	102.135
β/deg	90.526(2)	121	116.882	102.388 (12)	103.807(2)	90	106.334
γ/deg	90	90	90	90	90	90	97.4319
V/Å^3	10065.5(5)	3964.96(16)	12382.3 (8)	1729.1 (4)	2390.19(9)	3921.58(4)	1063.73(4)
D_{calcd}/(mg/m^3)	1.255	1.244	1.171	1.355	1.293	1.406	1.306
μ/mm^{-1}	0.489	3.393	0.405	0.491	0.376	5.330	0.409
F_{000}	4008	1560	4638	733	980	1712	442
total reflecns	24 234	6483	74 329	34 948	23 230	23 665	25 207
independ reflecns	16 354	4934	40 956	6087	11 055	6066	13 952
R_{int}	0.0369	0.0169	0.1277	0.1937	0.0381	0.0276	0.0239
data/restraints/param.	16354/1192/1208	4934/1/485	40 956/1818/1430	6087/37/453	11.055/14/590	6066/6/520	13 952/249/580
R1 $[I > 2\sigma(I)]$	0.0582	0.0367	0.0740	0.0487	0.0561	0.0290	0.0492
R_{w2}	0.1542	0.0951	0.1691	0.0990	0.1413	0.0784	0.1329
GoF on F_2	0.977	0.985	0.693	0.689	0.975	1.080	1.065
Z	4	4	4	2	2	4	1
T/K	100(2)	100(2)	100(2)	293(2)	100(2)	100(2)	100(2)
flack param	0.018(16)	0.005(4)	0.02(2)	0.05(3)	0.016(15)	0.006(3)	0.020(10)

$[\{FeL^{2}{}_{2}(\mu\text{-}C_{10}H_{8}N_{2})\}_{\infty}]$. To a stirred solution of $[FeL^{2}{}_{2}]$ (0.308 g, 0.5 mmol) in Et_2O (20 mL) was added 4,4′-bipyridine (0.08 g, 0.5 mmol) in Et_2O (10 mL) via cannula. The mixture was stirred for 15 min and concentrated to ca. 5 mL. Single crystals were grown in acetonitrile upon standing at −30 °C for 1 week (0.31 g, 80%). IR (cm^{-1}): 1618 m, 1527, 1329, 1267, 1250, 1212, 1177, 1143, 1055, 828, 746, 699 w. Anal. Found (calcd for $C_{48}H_{52}FeN_4O_2$; %): C, 74.50 (74.60); H, 6.80 (6.78); N, 7.70 (7.25). UV in MeCN (λ, nm (ε, M^{-1} cm^{-1})): 236 (76 000), 265 (75 000), 334 (20 000).

$[\{FeL^{3}{}_{2}(\mu\text{-}C_{4}H_{4}N_{2})\}_{\infty}]$. To a solution of $[FeL^{3}{}_{2}]$ (0.297 g, 0.5 mmol) in THF (10 mL) was added pyrazine (0.04 g, 0.5 mmol) in THF (10 mL) via cannula. The mixture was then allowed to stir overnight. The solvent was removed in vacuo to induce crystallization. The product was isolated by filtration. Single crystals were grown by slow cooling of a hot acetonitrile solution. (0.22 g, 65%). IR (cm^{-1}): 1607 m (NO_2), 1539, 1335, 1261, 1192, 1149, 1126, 1079, 1040, 970, 947, 930, 807, 722, 700 w. Anal. Found (calcd for $C_{34}H_{30}FeN_6O_6$; %): C, 60.31 (60.54); H, 4.49 (4.48); N, 12.23 (12.46). UV in MeCN (λ, nm (ε, M^{-1} cm^{-1})): 233 (90 000), 259 (78 000), 355 (27 000), 480 sh (6000).

$[\{FeL^{3}{}_{2}(\mu\text{-}C_{10}H_{8}N_{2})\}_{\infty}]\cdot$THF. To a solution of $[FeL^{3}{}_{2}]$ (0.297 g, 0.5 mmol) in THF (10 mL) was added 4,4′-bipyridine (0.08 g, 0.5 mmol) in THF (10 mL) via cannula. The mixture was then allowed to stir overnight. The solvent was removed in vacuo to induce crystallization. The product was isolated by filtration (0.25 g, 61%). Single crystals were grown in THF upon standing at −5 °C for 1 week. IR (cm^{-1}): 1598 m (NO_2), 1547, 1532 w, 1309 m (NO_2), 1242, 1102, 946, 805, 757, 697 w. Anal. Found (calcd for $C_{44}H_{42}FeN_6O_7$; %): C, 64.38 (64.24); H, 4.93 (5.15); N, 10.00 (10.22). UV in MeCN (λ, nm (ε, M^{-1} cm^{-1})): 234 (71 000), 371 (39 000), 500 sh (7000).

$[\{FeL^{4}{}_{2}(\mu\text{-}C_{4}H_{4}N_{2})\}_{\infty}]$. To a stirred red solution of $[FeL^{4}{}_{2}]$ (0.282 g, 0.5 mmol) in Et_2O (20 mL) was added a colorless solution of pyrazine (0.04 g, 0.5 mmol) in Et_2O (10 mL) via cannula. The mixture was stirred for 15 min and then concentrated to ca. 10 mL. The compound crystallized as purple needles over 12 h. The crystals were isolated by filtration and dried in vacuo for 2 h (0.22 g, 68%). IR (cm^{-1}): 1601 m, 1540, 1316, 1301, 1254, 121, 1157, 1079, 1042, 917, 815, 794, 721 w. Anal. Found (calcd for $C_{36}H_{36}FeN_4O_4$; %): C, 66.90 (67.08); H, 5.60 (5.63); N, 8.60 (8.69). UV in MeCN (λ, nm (ε, M^{-1} cm^{-1})): 236 (80 000), 378 (21 000), 500 sh (7000).

$[\{FeL^{4}{}_{2}(\mu\text{-}C_{10}H_{8}N_{2})\}_{\infty}]$. To a stirred red solution of $[FeL^{4}{}_{2}]$ (0.282 g, 0.5 mmol) in Et_2O (20 mL) was added a colorless solution of 4,4′-bipyridine (0.08 g, 0.5 mmol in Et_2O (10 mL) via cannula. The mixture was stirred for 15 min and then concentrated to ca. 10 mL. The compound crystallized as purple needles over 12 h. The crystals were isolated by filtration and dried in vacuo for 2 h (0.30 g, 83%). IR (cm^{-1}): 1597 m, 1537, 1320, 1256, 1215, 1156, 1041, 811, 721 w. Anal. Found (calcd for $C_{42}H_{40}FeN_4O_4$; %): C, 69.45 (70.00); H, 5.41 (5.59); N, 7.73 (7.77). UV in MeCN (λ, nm (ε, M^{-1} cm^{-1})): 236 (79 000), 377 (29 000), 500 sh (7000).

$[\{FeL^{5}{}_{2}(\mu\text{-}C_{4}H_{4}N_{2})\}_{\infty}]\cdot 0.5CH_3OH$. To a stirred red solution of $[FeL^{5}{}_{2}]$ (0.277 g, 0.5 mmol) in methaol (20 mL) was added a colorless solution of pyrazine (0.04 g, 0.5 mmol) in methanol (10 mL) via cannula. The mixture was stirred for 15 min and then concentrated to ca. 10 mL. The compound crystallized as purple needles over 12 h. The crystals were isolated by filtration and dried in vacuo for 2 h (0.19 g, 58%). IR (cm^{-1}): 2207 m (CN), 1605 m, 1524, 1482, 1349, 1261, 1210, 1156, 1041, 822, 721 w. Anal. Found (calcd for $C_{36.5}H_{32}FeN_6O_{2.5}$; %): C, 67.36 (67.39); H, 4.79 (4.96); N, 12.87 (12.92). UV in MeCN (λ, nm (ε, M^{-1} cm^{-1})): 244 (76 000), 286 (26 000), 341 (12 000), 500 sh (2000).

$[\{FeL^{5}{}_{2}(\mu\text{-}C_{10}H_{8}N_{2})\}_{\infty}]\cdot$THF. To a stirred red solution of $[FeL^{5}{}_{2}]$ (0.277 g, 0.5 mmol) in THF (20 mL) was added a colorless solution of 4,4′-bipyridine (0.08 g, 0.5 mmol) in THF (10 mL) via cannula. The mixture was stirred for 15 min and then concentrated to ca. 10 mL. The compound crystallized as purple needles over 12 h and dried in vacuo for 2 h (0.26 g, 66%). The single crystals were grown by slow cooling of hot $CHCl_3$ solution. IR (cm^{-1}): 2214 m (CN), 1605, 1526, 1486, 1351, 1262, 1214, 1157, 1135, 1068, 827, 722 w. Anal. Found (calcd for $C_{46}H_{42}FeN_6O_3$; %): C, 70.36 (70.59); H, 5.44 (5.41); N, 10.76 (10.74). UV in MeCN (λ, nm (ε, M^{-1} cm^{-1})): 237 (66 000), 243 (66 000), 284 (20 000), 336 (11 000), 500 sh (1000).

$[\{FeL^{6}(\mu\text{-}C_{10}H_{8}N_{2})\}_{\infty}]\cdot$2THF. To a stirred red solution of $[FeL^{6}{}_{2}]$ (0.268 g, 0.5 mmol) in THF (20 mL) was added a colorless solution of 4,4′-bipyridine (0.08 g, 0.5 mmol) in THF (10 mL) via cannula. The mixture was stirred for 15 min and then concentrated to ca. 10 mL. The compound precipitated as purple solid immediately. The crystals were isolated by filtration and dried in vacuo for 2 h (0.30 g, 72%). The single crystals were grown in THF solution at room temperature for 1 week. IR (cm^{-1}): 3300 m (O−H), 1593, 1553, 1535, 1404, 1260, 1212, 1152, 1078, 1050, 820, 721 w. Anal. Found (calcd for $C_{48}H_{52}FeN_4O_6$; %): C, 67.95 (68.90); H, 6.00 (6.26); N, 6.87 (6.70). UV in MeCN (λ, nm (ε, M^{-1} cm^{-1})): 234 (80 000), 260 (60 000), 344 (27 000).

■ ASSOCIATED CONTENT

Ⓢ Supporting Information. Figures showing crystallography and χ_M and $\chi_M T$ and text describing the analysis of magnetic data, CIF data. This material is available free of charge via the Internet at http://pubs.acs.org.

■ AUTHOR INFORMATION

Corresponding Author

*E-mail: peter.scott@warwick.ac.uk. Tel.: 024 7652 3238. Fax: 024 7657 2710.

■ ACKNOWLEDGMENT

We thank the University of Warwick for a Warwick Postgraduate Research Fellowship (L.L.) and EPSRC for support (L.E.N.A.). The Oxford Diffraction Gemini XRD system was obtained through the Science City Advanced Materials project: Creating and Characterizing Next Generation Advanced Materials project, with support from Advantage West Midlands (AWM) and part funded by the European Regional Development Fund (ERDF).

■ REFERENCES

(1) Kahn, O. *Molecular Magnetism*; Wiley-VCH: New York, 1993.

(2) Janiak, C. *Dalton Trans.* **2003**, 2781.

(3) Slinker, J.; Bernards, D.; Houston, P. L.; Abruna, H. D.; Bernhard, S.; Malliaras, G. G. *Chem. Commun. (Cambridge, U. K.)* **2003**, 2392.

(4) Ohkoshi, S.; Tokoro, H.; Matsuda, T.; Takahashi, H.; Irie, H.; Hashimoto, K. *Angew. Chem., Int. Ed.* **2007**, *46*, 3238.

(5) Xu, G.-C.; Ma, X.-M.; Zhang, L.; Wang, Z.-M.; Gao, S. *J. Am. Chem. Soc.* **2010**, *132*, 9588.

(6) Jain, P.; Ramachandran, V.; Clark, R. J.; Zhou, H. D.; Toby, B. H.; Dalal, N. S.; Kroto, H. W.; Cheetham, A. K. *J. Am. Chem. Soc.* **2009**, *131*, 13625.

(7) Kahn, O.; Codjovi, E. *Philos. Trans. R. Soc. London, Ser. A* **1996**, *354*, 359.

(8) Kahn, O.; Garcia, Y.; Létard, J.-F.; Mathoniére, C. Hysteresis and memory effect in supramolecular chemistry. In *NATO ASI Series C*; Supramolecular Engineering of Synthetic Metallic Materials: Conductors and Magnets; Kluwer Academic Publishers: Dordrecht, 1999; p 127.

(9) Zhang, D.; Wang, H.; Tian, L.; Kou, H.-Z.; Jiang, J.; Ni, Z.-H. *Cryst. Growth Des.* **2009**, *9*, 3989.

(10) Colacio, E.; Ghazi, M.; Stoeckli-Evans, H.; Lloret, F.; Moreno, J. M.; Pérez, C. *Inorg. Chem.* **2001**, *40*, 4876.

(11) Hursthouse, M. B.; Light, M. E.; Price, D. J. *Angew. Chem., Int. Ed.* **2004**, *43*, 472.

(12) Keene, T.; Ogilvie, H.; Hursthouse, M.; Price, D. *Eur. J. Inorg. Chem.* **2004**, *2004*, 1007.

(13) Tamaki, H.; Zhong, Z. J.; Matsumoto, N.; Kida, S.; Koikawa, M.; Achiwa, N.; Hashimoto, Y.; Okawa, H. *J. Am. Chem. Soc.* **1992**, *114*, 6974.

(14) Li, W.; Jia, H. P.; Ju, Z. F.; Zhang, J. *Dalton Trans.* **2008**, 5350.

(15) Zheng, Y.-Z.; Xue, W.; Tong, M.-L.; Chen, X.-M.; Grandjean, F.; Long, G. J. *Inorg. Chem.* **2008**, *47*, 4077.

(16) Konar, S.; Zangrando, E.; Drew, M. G. B.; Mallah, T.; Ribas, J.; Chaudhuri, N. R. *Inorg. Chem.* **2003**, *42*, 5966.

(17) Gu, Z.-G.; Xu, Y.-F.; Yin, X.-J.; Zhou, X.-H.; Zuo, J.-L.; You, X.-Z. *Dalton Trans.* **2008**, 5593.

(18) Tang, L.-F.; Zhang, L.; Li; Cheng, P.; Wang, Z.-H.; Wang, J.-T. *Inorg. Chem.* **1999**, *38*, 6326.

(19) Gao, E.-Q.; Bai, S.-Q.; Yue, Y.-F.; Wang, Z.-M.; Yan, C.-H. *Inorg. Chem.* **2003**, *42*, 3642.

(20) Wen, H.-R.; Wang, C.-F.; Song, Y.; Zuo, J.-L.; You, X.-Z. *Inorg. Chem.* **2005**, *44*, 9039.

(21) Wriedt, M.; Jess, I.; Näther, C. *Eur. J. Inorg. Chem.* **2009**, *2009*, 1406.

(22) Bordallo, H. N.; Chapon, L.; Manson, J. L.; Ling, C. D.; Qualls, J. S.; Hall, D.; Argyriou, D. N. *Polyhedron* **2003**, *22*, 2045.

(23) Moliner, N.; Muñoz, M. C.; Létard, S.; Salmon, L.; Tuchagues, J.-P.; Bousseksou, A.; Real, J. A. *Inorg. Chem.* **2002**, *41*, 6997.

(24) Genre, C.; Matouzenko, G. S.; Jeanneau, E.; Luneau, D. *New J. Chem.* **2006**, *30*, 1669.

(25) Le Goff, X. F.; Willemin, S.; Coulon, C.; Larionova, J.; Donnadieu, B.; Clérac, R. *Inorg. Chem.* **2004**, *43*, 4784.

(26) Tancharakorn, S.; Fabbiani, F. P. A.; Allan, D. R.; Kamenev, K. V.; Robertson, N. *J. Am. Chem. Soc.* **2006**, *128*, 9205.

(27) Murrie, M.; Price, D. J. *Annu. Rep. Prog. Chem., Sect. A: Inorg. Chem.* **2007**, *103*, 20–38.

(28) Roques, N.; Maspoch, D.; Imaz, I.; Datcu, A.; Sutter, J.-P.; Rovira, C.; Veciana, J. *Chem. Commun. (Cambridge, U. K.)* **2008**, 3160.

(29) Roesky, H. W.; Andruh, M. *Coord. Chem. Rev.* **2003**, *236*, 91.

(30) Xiang, H.; Wang, S.-J.; Jiang, L.; Feng, X.-L.; Lu, T.-B. *Eur. J. Inorg. Chem.* **2009**, *2009*, 2074.

(31) Sun, H.-L.; Wang, Z.-M.; Gao, S. *Inorg. Chem.* **2005**, *44*, 2169.

(32) Triki, S.; Bérézovsky, F.; Sala Pala, J.; Gómez-García, C. J.; Coronado, E.; Costuas, K.; Halet, J.-F. *Inorg. Chem.* **2001**, *40*, 5127.

(33) Manson, J. L.; Gu, J.; Schlueter, J. A.; Wang, H. H. *Inorg. Chem.* **2003**, *42*, 3950.

(34) Train, C.; Gheorghe, R.; Krstic, V.; Chamoreau, L.-M.; Ovanesyan, N. S.; Rikken, G. L. J. A.; Gruselle, M.; Verdaguer, M. *Nat. Mater.* **2008**, *7*, 729.

(35) Rikken, G. L. J. A.; Fölling, J.; Wyder, P. *Phys. Rev. Lett.* **2001**, *87*, 236602.

(36) Coronado, E.; Galán-Mascarós, J. R.; Gómez-García, C. J.; Murcia-Martínez, A. *Chem.—Eur. J.* **2006**, *12*, 3484.

(37) Beghidja, A.; Rabu, P.; Rogez, G.; Welter, R. *Chem.—Eur. J.* **2006**, *12*, 7627.

(38) Beghidja, A.; Rogez, G.; Welter, R.; Drillon, M. *J. Mater. Chem.* **2006**, *16*, 2715.

(39) Becker, J. M.; Barker, J.; Clarkson, G. J.; Gorkum, R. v.; Johal, G. K.; Walton, R. I.; Scott, P. *Dalton Trans.* **2010**, *39*, 2309.

(40) Norman, F. M. Henpy, K. l. *International Tables for X-ray Cryatallography*; International Union of Crystallography: Kynoch Press, Birmingham, U. K., 1965.

(41) Gutlich, P.; Garcia, Y.; Goodwin, H. A. *Chem. Soc. Rev.* **2000**, *29*, 419.

(42) Manna, S. C.; Zangrando, E.; Ribas, J.; Ray Chaudhuri, N. *Inorg. Chim. Acta* **2005**, *358*, 4497.

(43) Fisher, M. E. *J. Phys. (Paris)* **1964**, *32*, 343.

(44) Bain, G. A.; Berry, J. F. *J. Chem. Educ.* **2008**, *85*, 532.